Near Field Propulsion Forces from Nonreciprocal Media

David Gelbwaser-Klimovsky, 1,* Noah Graham, Mehran Kardar, and Matthias Krüger. 4

1 Physics of Living Systems, Department of Physics, Massachusetts Institute of Technology, Cambridge, Massachusetts 02139, USA

2 Department of Physics, Middlebury College, Middlebury, Vermont 05753 USA

3 Department of Physics, Massachusetts Institute of Technology, Cambridge, Massachusetts 02139, USA

4 Institute for Theoretical Physics, Georg-August-Universität, 37077 Göttingen, Germany

(Received 5 January 2021; accepted 31 March 2021; published 28 April 2021)

Arguments based on symmetry and thermodynamics may suggest the existence of a ratchetlike lateral Casimir force between two plates at different temperatures and with broken inversion symmetry. We find that this is not sufficient, and at least one plate must be made of nonreciprocal material. This setup operates as a heat engine by transforming heat radiation into mechanical force. Although the ratio of the lateral force to heat transfer in the near field regime diverges inversely with the plates separation, d, an Onsager symmetry, which we extend to nonreciprocal plates, limits the engine efficiency to the Carnot value η_c . The optimal velocity of operation in the far field is of the order of $c\eta_c$, where c is the speed of light. In the near field regime, this velocity can be reduced to the order of $\bar{\omega} d\eta_c$, where $\bar{\omega}$ is a typical material frequency.

DOI: 10.1103/PhysRevLett.126.170401

Fluctuations of electromagnetic fields lead to a variety of phenomena, from Planck's law of thermal radiation [1], to the fluctuation-induced normal forces predicted by Casimir in 1948 [2] and later generalized by Lifshitz [3]. In 1971, Polder and van Hove discussed near field effects in radiative heat transfer between closely spaced objects [4], demonstrating a dramatic increase from the far field. These effects where observed experimentally for normal forces at the end of the last century [5,6], and roughly ten years later for radiative heat transfer [7–9]. A variety of related effects arise for Casimir forces in systems out of equilibrium [10–17], such as torques [18,19] and propulsion forces [20], in both near and far field regimes.

Lateral Casimir forces, which can propel plates with respect to each other, were also predicted between corrugated plates in equilibrium [21,22], and observed experimentally [23,24]. However, in these and several other equilibrium and nonequilibrium settings [20,25–27], either the shape or rotation of an object establishes the direction of the propulsive force. In contrast, we consider here a *translationally invariant object*, and demonstrate that a lateral (potentially propulsive) force can arise by taking advantage of radiative heat transfer involving *nonreciprocal* materials. Nonreciprocal media have indeed been shown to give rise to a variety of other interesting phenomena [28–31].

In this Letter, we demonstrate that nonequilibrium propulsive forces can be used to build a heat engine without any contact between its parts and whose optimal operation strongly depends on the type of radiation driving its heat transfer. In the far field limit, the on-shell photon energy-momentum relation bounds the ratio of propulsive force to heat transfer, requiring operational velocities of the

order of the speed of light, limiting the usefulness of such an engine. In the near field, the on-shell relation does not hold, allowing the engine to operate at efficiencies close to the Carnot bound at much lower velocities.

Consider the setup depicted in Fig. 1, with two objects held at different temperatures, characterized by reciprocal or nonreciprocal dielectric properties encoded in their scattering operators \mathbb{T}_i , where i=1,2. We are interested in propulsive or *motive forces* (MF) acting on object 2 in the y direction, along which it is translationally invariant. Such forces that may be used to drive an engine are ruled out for systems at thermal equilibrium, because we can then define a Casimir free energy, which does not change under a displacement of object 2 in the y direction.

For simplicity, let the temperatures of object 2 and of the environment be zero (this restriction will be relaxed below).

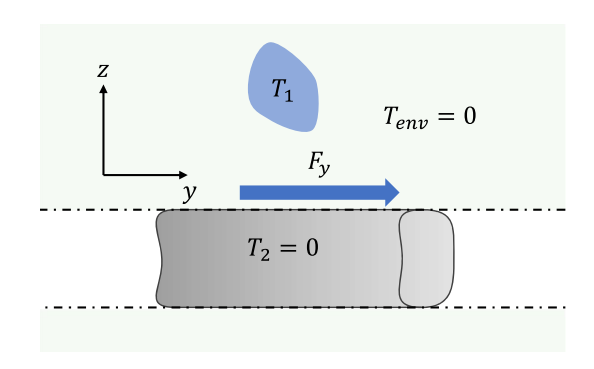


FIG. 1. Two objects placed in vacuum. Object 1 is held at temperature T_1 , while object 2 and the environment are held at zero temperature, for simplicity. Object 2 is translationally invariant in direction y, and we consider the force acting on it in that direction.

The y component of the force acting on object 2, F_y , can be derived using the techniques of Ref. [15], adapted to nonreciprocal media (see Supplemental Material [32]), and since \mathbb{T}_2 is not a function of y, we find

$$F_{y} = \frac{-2\hbar}{\pi} \int_{0}^{\infty} d\omega \frac{1}{e^{(\hbar\omega/k_{B}T_{1})} - 1} \operatorname{Tr}\{i\partial_{y}\mathbb{R}_{2}\mathbb{W}\mathbb{R}_{1}\mathbb{W}^{\dagger}\}. \tag{1}$$

Here we have introduced the radiation operators $\mathbb{R}_1 = \mathbb{G}_0\{[(\mathbb{T}_1 - \mathbb{T}_1^\dagger)/2i] - \mathbb{T}_1 \mathrm{Im}[\mathbb{G}_0]\mathbb{T}_1^\dagger\}\mathbb{G}_0^*, \quad \mathbb{R}_2 = \mathbb{G}_0^* \{[(\mathbb{T}_2 - \mathbb{T}_2^\dagger)/2i] - \mathbb{T}_2^\dagger \mathrm{Im}[\mathbb{G}_0]\mathbb{T}_2\}\mathbb{G}_0$ and the multiple scattering operator $\mathbb{W} = \mathbb{G}_0^{-1}(1 - \mathbb{G}_0\mathbb{T}_1\mathbb{G}_0\mathbb{T}_2)^{-1}$, where \mathbb{G}_0 is the free Green's function. The trace in Eq. (1) is understood to be taken over spatial coordinates as well as the indices of the 3×3 matrix [15]. Because of the translational invariance of object 2, $\mathbb{R}_2(y,y') = \mathbb{R}_2(y-y') = \int (dk_y/2\pi) \mathbb{R}_2(k_y) e^{ik_y(y-y')} = \int (dk_y/2\pi) \mathbb{R}_2$ can be decomposed in Fourier modes, and the force is written

$$F_{y} = \frac{2\hbar}{\pi} \int_{0}^{\infty} d\omega \frac{1}{e^{(\hbar\omega/k_{B}T_{1})} - 1} \int \frac{dk_{y}}{2\pi} k_{y} S(k_{y}). \tag{2}$$

Importantly, $S(k_y) = \text{Tr}\{\hat{\mathbb{R}}_2 \mathbb{W} \mathbb{R}_1 \mathbb{W}^{\dagger}\}$ is the *heat flux* density per wave vector k_y , and indeed the energy H absorbed by object 2 per unit time is given by

$$H = \frac{2\hbar}{\pi} \int_0^\infty d\omega \frac{\omega}{e^{\hbar\omega/k_B T_1} - 1} \int \frac{dk_y}{2\pi} S(k_y). \tag{3}$$

The objects are made of materials described by dielectric permittivity and magnetic permeability tensors $\boldsymbol{\epsilon}$ and $\boldsymbol{\mu}$, expressed in the potential $\mathbb{V}=(\omega^2/c^2)(\boldsymbol{\epsilon}-\mathbb{I})+\boldsymbol{\nabla}\times (\mathbb{I}-1/\boldsymbol{\mu})\boldsymbol{\nabla}\times$ [15]. For passive materials, $(\mathbb{V}-\mathbb{V}^\dagger)/i\geq 0$, which are local, $\mathbb{V}_2\sim\delta(y-y')$, one can prove that $\hat{\mathbb{R}}_2$ is positive semidefinite for any k_y (see Supplemental Material [32]), and

$$S(k_{y}) \ge 0. \tag{4}$$

Equation (4) implies that the heat flux is non-negative for any k_y (note that beyond passivity we have made no assumptions regarding the shape or properties of object 1). It also tells us that the force in Eq. (2) is due to absorbed photons, which contribute the y component of their momentum to the force. This property of MF, displayed in Eq. (2), tightly links MF and radiative energy transfer. This link, which is not present for other Casimir forces, has physical consequences: It leads, via Eq. (3), to a *bound* on the force from heat transfer, and also places restrictions on MF derived from thermodynamics, as discussed below.

In practice, the integral in Eq. (2) is often cut off by a maximal value k_y^{\max} (see below). With it, the spectral densities for F_y and H, $F_y \equiv \int_0^\infty d\omega f(\omega)$ and $H \equiv \int_0^\infty d\omega h(\omega)$, obey

$$|f(\omega)|c \le h(\omega)\frac{c}{\omega}k_y^{\max}.$$
 (5)

For on-shell modes, which are dominant in the far field, $k_v^{\text{max}} = \omega/c$, so

$$|f(\omega)|c \le h(\omega),\tag{6}$$

illustrating that MF are bounded by the photon energymomentum relation in this limit.

To find a bound in the near field, we consider two parallel, semi-infinite plates normal to z, separated by a distance d, as shown in Fig. 2. The force F_y in Eq. (2) can easily be extended to include nonzero T_2 ,

$$F_{y} = \frac{2\hbar}{\pi} \int_{0}^{\infty} d\omega (n_1 - n_2) \int \frac{dk_y}{2\pi} k_y S(k_y), \qquad (7)$$

with $n_i = (e^{(\hbar\omega/k_BT_i)} - 1)^{-1}$. Here, $S(k_y)$ is the heat flux between the two plates of surface area A, given by [36]

$$\begin{split} \frac{S(k_y)}{A} &= \int \frac{dk_x}{8\pi} \{ \mathrm{Tr}_p[(1-\mathbf{r}_2^\dagger \mathbf{r}_2) \mathbb{D}(1-\mathbf{r}_1\mathbf{r}_1^\dagger) \mathbb{D}^\dagger] \Theta_{pr} \\ &+ e^{-2|k_z|d} \mathrm{Tr}_p[(\mathbf{r}_2^\dagger - \mathbf{r}_2) \mathbb{D}(\mathbf{r}_1 - \mathbf{r}_1^\dagger) \mathbb{D}^\dagger] \Theta_{ev} \}, \quad (8) \end{split}$$

where $\mathbb{D} = (1 - \mathbb{r}_1 \mathbb{r}_2 e^{2ik_z d})^{-1}$ and \mathbb{r}_i is the Fresnel reflection tensor of plate i: a 2×2 matrix in the space of polarizations [9] with the trace taken in that space. We have introduced projectors Θ_{pr} and Θ_{ev} for propagating and evanescent modes, respectively. Equation (8) holds for reciprocal or nonreciprocal plates, and in general \mathbb{r}_i has off-diagonal elements that couple the polarizations.

The constraints for motion in asymmetric ratchet systems out of equilibrium has been a subject of intense research in recent years [37–43]. (The Feynman ratchet does not rotate in equilibrium, but does when heated [44].) We may thus expect that if the plates in Fig. 2 are not symmetric under $y \rightarrow -y$, e.g., for a tensorial dielectric response with tilted axes, a nonequilibrium heat flux will be generically accompanied by a ratchetlike MF. Surprisingly, this is not the case for asymmetric, but reciprocal plates: As shown in Ref. [45] by explicit manipulations of Eq. (8), $S(k_y)$ is symmetric in k_y if the two plates are made of

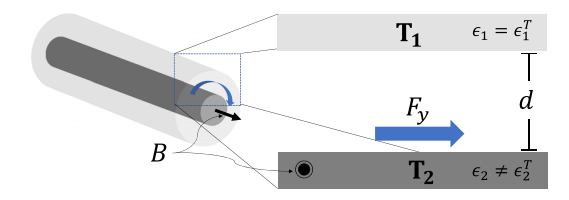


FIG. 2. Two parallel plates at a distance *d*, at different temperatures. At close proximity, these may mimic, e.g., inner and outer parts of an engine axis (left). We consider the case where the lower plate is nonreciprocal, which may, e.g., be due to a magnetic field pointing in the direction as indicated in the figure.

reciprocal materials. We extended this unexpected observation to arbitrary objects that are translationally invariant in direction y (see Supplemental Material [32]), and conclude that nonreciprocity is necessary for near field MF. Furthermore, translational symmetry is an important element: If object 1 is not translationally invariant, Eq. (2) can yield a finite result for reciprocal media, as was found for an ellipsoid near a planar surface [20].

Assuming that at least one of the plates is nonreciprocal, we investigate the distance dependence of the force. For small separations, the integral over k_x and k_y in Eq. (7) is dominated by the evanescent sector for large values of $k_{\perp} = \sqrt{k_x^2 + k_y^2} \sim 1/d$. We can thus expand the reflection tensors for large k_{\perp} . In particular, we consider a dielectric tensor of the form

$$\boldsymbol{\epsilon} = \begin{pmatrix} \epsilon_p & 0 & 0 \\ 0 & \epsilon_d & -i\epsilon_f \\ 0 & i\epsilon_f & \epsilon_d \end{pmatrix}, \tag{9}$$

which is realized in magneto-optical materials with a dc magnetic field pointing along the x direction [46]. For $k_\perp^2 \gg (\omega^2/c^2)|\varepsilon_{ij}|$, the reflection tensor becomes diagonal, and is dominated by the entry for electric polarization, r^{NN} . Denoting, in this limit, $r^{NN} \equiv r^{\infty}$, we find (using $k_y = k_\perp \sin \theta$) (see Supplemental Material [32])

$$r^{\infty} = \frac{(\epsilon_d - 1) + \sin \theta \epsilon_f}{(\epsilon_d + 1) + \sin \theta \epsilon_f}.$$
 (10)

By making k_{\perp} dimensionless, $\tilde{k}_{\perp} = k_{\perp}d$, in the limit where d is small compared to all other length scales, such as the thermal wavelength, and the material skin depth, we obtain

$$\frac{F_{y}}{A} = \frac{2\hbar}{\pi d^{3}} \int_{0}^{\infty} d\omega (n_{1} - n_{2})
\int \frac{d^{2}\tilde{k}_{\perp}}{(2\pi)^{2}} \tilde{k}_{y} \frac{e^{-2|\tilde{k}_{\perp}|} \text{Im}[r_{2}^{\infty}] \text{Im}[r_{1}^{\infty}]}{|1 - r_{1}^{\infty}r_{2}^{\infty}e^{-2|\tilde{k}_{\perp}|}|^{2}}.$$
(11)

The force in Eq. (11) is of similar form as normal forces of thermal origin [10], and we expect it to be of experimental relevance, depending on materials used (see Supplemental Material [32]); it diverges as d^{-3} for small separations d. The well-known fact that heat transfer H diverges as d^{-2} in the same limit, which can easily be confirmed here by using the same rescaling with Eq. (10), implies that the ratio between force and heat transfer is proportional to d^{-1} . To quantify this, we compute $f(\omega, \theta)$ and $h(\omega, \theta)$, the force and heat transfer per frequency and per angle θ in the $k_x k_y$ plane. The integral over $|k_\perp|$ can then be performed to yield

$$f(\omega, \theta)c = h(\omega, \theta) \frac{c}{\omega d} \sin \theta g[r_1^{\infty}(\theta) r_2^{\infty}(\theta)], \quad (12)$$

where g(x) is a well-behaved positive function, which approaches unity for $|x| \to 0$, which corresponds to dilute materials [47].

Equation (12) may also be understood from Eq. (5): The integral of \tilde{k}_y is limited by the exponential terms, implying $\tilde{k}_y^{\rm max} \approx 1$.

Using the mediant inequality yields, after integration over θ , a bound valid for small distance d: in terms of the maximum of $|\sin \theta|g$ as a function of θ ,

$$\frac{|f(\omega)|c}{h(\omega)\max(|\sin\theta|g)} \le \frac{c}{\omega d}.$$
 (13)

Equation (13) is a notable extension of Eq. (6). In the near field, the force is also bounded by the heat transfer, but the bound diverges as $d \to 0$, since there is no longer any energy–momentum relation constraining evanescent waves.

As a particular example, we consider that plate 1 is composed of the reciprocal material SiC (with dielectric properties taken from Ref. [48]), and plate 2 made of n-doped InSb under the influence of a magnetic field along the x axis. The entries of ϵ in Eq. (9) are given by [28] $\epsilon_d = 1 - \{[\omega_p^2(1+i\omega_\tau/\omega)]/[(\omega+i\omega_\tau)^2-\omega_b^2]\}, \ \epsilon_p = 1-\omega_p^2/\omega(\omega+i\omega_\tau), \ \text{and} \ \epsilon_f = -\{[\omega_b\omega_p^2]/[\omega((\omega+i\omega_\tau)^2-\omega_b^2)]\}.$

Here, ω_p is the plasma frequency and ω_{τ} describes relaxation effects in InSb; the nonreciprocity ($\epsilon_f \neq 0$) due to the magnetic field is encoded via the cyclotron frequency ω_b .

Using material parameters tabulated in the Supplemental Material [32], Fig. 3 depicts F_yc and H plotted as functions of separation d. As required by Eq. (5), the magnitude of F_yc is smaller than H in the far field. For distances below ~ 100 nm, a steeper divergence of F_y is observed, so that the two quantities cross at roughly 30 nm. For smaller separations, the on-shell energy–momentum relation of photons is noticeably broken. This crossing point depends on the nonreciprocal properties of the materials, which in turn depend on the strength of the magnetic field[49]. The inset of Fig. 3 shows the left-hand side of Eq. (13) for the given materials as a function of frequency. It confirms the inequality of Eq. (13), and that it presents a realistic bound, with some points reaching close to the bound.

Acting as a heat engine in a setup such as in Fig. 2, the force F_y can be used to extract work from the heat H by moving the plate at a velocity v along the y direction. The extracted power is given by $P = F_y v + \mathcal{O}(v^2)$, yielding to leading order in v, the efficiency

$$\eta = \frac{F_y}{H}v + \mathcal{O}(v^2). \tag{14}$$

Prima facie, this expression suggests a Carnot efficiency, $\eta_c = \Delta T/T_1$ where $T_1 - T_2 = \Delta T > 0$, at $v_c = (H/F_y)\eta_c$, and exceeding it for larger velocities. However, as shown

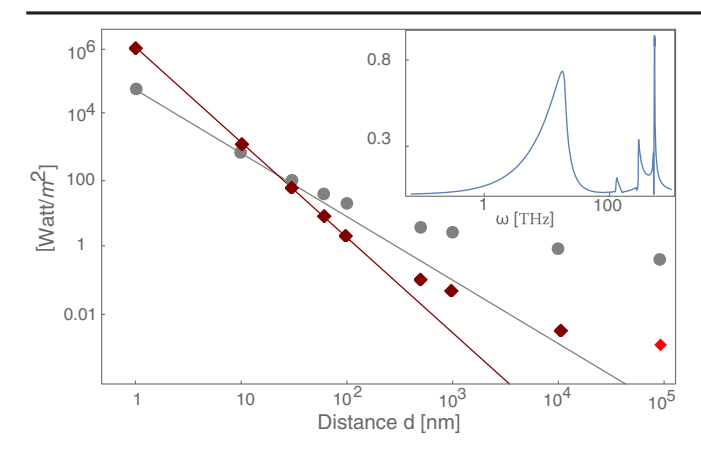


FIG. 3. Scaled motive force F_yc (red diamonds), and heat transfer H (gray circles) for a SiC plate and one of n-InSb subject to a magnetic field along the x axis. The dots correspond to numeric calculations and the continuous lines to the small d asymptotes from Eq. (11) and its equivalent for H. Note that the force changes sign from +y to -y (dark red to light red diamond) at large separation. Inset: left-hand side of Eq. (13) in units of $c/(\omega d)$ for d=1 nm. Figures' parameters: B=10T, $T_1=300K$, $T_2=270K$.

below, for $v \sim v_c$ one cannot neglect $\mathcal{O}(v^2)$ terms. Nonetheless, the first-order analysis provides an estimate of the scale at which efficiency is maximal. In the far field, Eq. (6) implies that v_c is larger than $\eta_c c$, while in the near field, Eq. (13) shows that it can be much smaller, going to zero linearly with d.

When running at velocities $v \sim v_c$, both force and heat exchange become functions of velocity, so that higher order terms in Eq. (14) arise. While computing them poses no problem in principle, we restrict our discussion here to the limit of small $\Delta T \ll T_1$, where Onsager symmetry relations allow for some insights. While these relations rely on time-reversal symmetry in general, we find them to also be valid for nonreciprocal plates, leading to a modification of heat transfer between the plates, as

$$\mathcal{H} = H + \frac{T_1}{\Delta T} F_y v + \mathcal{O}(v^2) = H \left[1 + \frac{v}{v_c} + \mathcal{O}(v^2) \right]. \tag{15}$$

The Onsager's relation leading to Eq. (15) ensures that η remains below the Carnot limit. Interestingly, Eq. (15) indicates that the given setup can also act as a refrigerator [50]: A backward velocity of order $-v_c$ can remove heat from the cold plate.

There is also an $\mathcal{O}(v)$ reduction to MF from friction due to fluctuations of the electromagnetic field, reducing the engine power to $P = v[F_y - \Gamma v + \mathcal{O}(v^2)]$, where we have introduced the friction coefficient Γ , relating force and velocity at $\Delta T = 0$. It is given by a generalization of the result for reciprocal media [51,52] as

$$\frac{\Gamma}{A} = -\frac{2\hbar}{\pi} \int_0^\infty d\omega \frac{\partial n_1}{\partial \omega} \int \frac{dk_y}{2\pi} k_y^2 S(k_y) \ge 0, \quad (16)$$

with $S(k_y)$ given in Eq. (8), so that $\Gamma \ge 0$. Expanding Eq. (16) for small d as in Eq. (11), and using Eq. (10), leads to a $1/d^4$ divergence. Comparing Γv to F_y , one may thus expect the velocity scale v_c to reappear.

As a simple illustration, let us consider two dilute materials with r_1^{∞} , $r_2^{\infty} \to 0$, and assume that the response of the nonreciprocal medium is focused at a single frequency \bar{o} , such that [53]

$$\operatorname{Im}[r_2^{\infty}](\omega) = r_n(1 + \alpha \sin \theta + \cdots) \bar{\omega} \, \tilde{\delta}(\omega - \bar{\omega}). \tag{17}$$

The parameter α is a dimensionless measure of influence of nonreciprocity on the reflection coefficient, and r_n a unitless prefactor; the requirement that the material be passive implies $\text{Im}[r_2^\infty] \geq 0$, and hence $|\alpha| \leq 1$ in absence of higher-order terms. This form yields

$$\frac{F_y}{A} = C \frac{\alpha \eta_c \hbar \bar{\omega}}{d^3}, \qquad \frac{H}{A} = 2C \frac{\eta_c \hbar \bar{\omega}^2}{d^2}, \qquad \frac{\Gamma}{A} = \frac{3}{2} C \frac{\hbar}{d^4}, \tag{18}$$

where $C = -(\bar{\omega}/8\pi^2)(\partial n_1/\partial \bar{\omega})r_n \text{Im}[r_1^{\infty}]$. This leads to a velocity scale $v_c = \eta_c(2\bar{\omega}d/\alpha)$, and an efficiency

$$\eta = \eta_c \frac{v}{v_c} \frac{1 - 3v/(\alpha^2 v_c) + \dots}{1 + v/v_c + \dots}.$$
 (19)

We expect higher-order terms in Eq. (15) to become important for $v \sim \bar{\omega}d$. However, the velocity scale v_c carries an additional factor of η_c , which allows us to ignore higher order terms for $\Delta T \ll T_1$. Equation (19) then gives that velocity at maximum power as $v_{MP} = \alpha^2 v_c/6 = \alpha \eta_c \bar{\omega}d/3$, at which point the efficiency is $\eta_{MP} = \eta_c [\alpha^2/2(6 + \alpha^2)]$.

In summary, we have shown that for the case of two smooth plates at different temperatures, nonequilibrium fluctuations will cause a motive force if at least one of the plates is made of a nonreciprocal material. Although for large plate separation the on-shell energy-momentum photon relation limits the ratio between motive force and heat transfer, at small separations, the heat transfer and propulsion force are dominated by evanescent modes, allowing this ratio to grow inversely with the distance between the two plates. The velocity scale corresponding to maximal efficiency and power is thus linear in that distance.

It is a pleasure to thank G. Bimonte, T. Emig, and R. L. Jaffe for helpful conversations. D. G. K. is supported by the Gordon and Betty Moore Foundation as Physics of Living Systems Fellows through Grant No. GBMF4513. N. G. was supported in part by the National Science Foundation (NSF) through Grant No. PHY-1820700. M. K.

acknowledges support from the NSF through Grant No. DMR-1708280.

- *Corresponding author. dgelbi@mit.edu
- [1] M. Planck, Ann. Phys. (Leipzig) 4, 553 (1901).
- [2] H. B. Casimir, Proc. Kon. Ned. Akad. Wet. **51**, 793 (1948).
- [3] E. Lifshitz, J. Exp. Theor. Phys. 2, 73 (1956).
- [4] D. Polder and M. Van Hove, Phys. Rev. B 4, 3303 (1971).
- [5] S. K. Lamoreaux, Phys. Rev. Lett. 78, 5 (1997).
- [6] U. Mohideen and A. Roy, Phys. Rev. Lett. **81**, 4549 (1998).
- [7] S. Shen, A. Narayanaswamy, and G. Chen, Nano Lett. 9, 2909 (2009).
- [8] E. Rousseau, A. Siria, G. Jourdan, S. Volz, F. Comin, J. Chevrier, and J.-J. Greffet, Nat. Photonics 3, 514 (2009).
- [9] S.-A. Biehs, R. Messina, P. S. Venkataram, A. W. Rodriguez, J. C. Cuevas, and P. Ben-Abdallah, arXiv:2007.05604.
- [10] M. Antezza, L. P. Pitaevskii, S. Stringari, and V. B. Svetovoy, Phys. Rev. A 77, 022901 (2008).
- [11] G. Bimonte, Phys. Rev. A 80, 042102 (2009).
- [12] R. Messina and M. Antezza, Europhys. Lett. 95, 61002 (2011).
- [13] M. Krüger, T. Emig, and M. Kardar, Phys. Rev. Lett. 106, 210404 (2011).
- [14] R. Messina and M. Antezza, Phys. Rev. A 84, 042102 (2011).
- [15] M. Krüger, G. Bimonte, T. Emig, and M. Kardar, Phys. Rev. B 86, 115423 (2012).
- [16] A. Narayanaswamy and Y. Zheng, J. Quant. Spectrosc. Radiat. Transfer 132, 12 (2014), special issue on Micro- and Nano-Scale Radiative Transfer.
- [17] G. Bimonte, T. Emig, M. Kardar, and M. Krüger, Annu. Rev. Condens. Matter Phys. **8**, 119 (2017).
- [18] M. T. H. Reid, O. Miller, A. Polimeridis, A. Rodriguez, E. Tomlinson, and S. Johnson, arXiv:1708.01985.
- [19] Y. Guo and S. Fan, arXiv:2007.11234.
- [20] B. Müller and M. Krüger, Phys. Rev. A 93, 032511 (2016).
- [21] R. Golestanian and M. Kardar, Phys. Rev. Lett. **78**, 3421 (1997).
- [22] T. Emig, A. Hanke, R. Golestanian, and M. Kardar, Phys. Rev. Lett. 87, 260402 (2001).
- [23] F. Chen, U. Mohideen, G. L. Klimchitskaya, and V. M. Mostepanenko, Phys. Rev. Lett. 88, 101801 (2002).
- [24] A. A. Banishev, J. Wagner, T. Emig, R. Zandi, and U. Mohideen, Phys. Rev. Lett. 110, 250403 (2013).
- [25] A. Ashourvan, M. F. Miri, and R. Golestanian, Phys. Rev. Lett. 98, 140801 (2007).
- [26] H.-C. Chiu, G. L. Klimchitskaya, V. N. Marachevsky, V. M. Mostepanenko, and U. Mohideen, Phys. Rev. B 81, 115417 (2010).

- [27] S. A. H. Gangaraj, G. W. Hanson, M. Antezza, and M. G. Silveirinha, Phys. Rev. B 97, 201108(R) (2018).
- [28] L. Zhu and S. Fan, Phys. Rev. Lett. 117, 134303 (2016).
- [29] F. Herz and S.-A. Biehs, Europhys. Lett. 127, 44001 (2019).
- [30] I. Latella and P. Ben-Abdallah, Phys. Rev. Lett. 118, 173902 (2017).
- [31] P. Ben-Abdallah, Phys. Rev. Lett. 116, 084301 (2016).
- [32] See Supplemental Material at http://link.aps.org/supplemental/ 10.1103/PhysRevLett.126.170401, which includes Refs. [33– 35], for more details on the derivations as well as comparison with experimental capabilities.
- [33] H. C. Chen, Radio Sci. 16, 1213 (1981).
- [34] R. S. Decca, D. López, E. Fischbach, G. L. Klimchitskaya, D. E. Krause, and V. M. Mostepanenko, Phys. Rev. D 75, 077101 (2007).
- [35] S. Law, R. Liu, and D. Wasserman, J. Vac. Sci. Technol. B 32, 052601 (2014).
- [36] E. Moncada-Villa, V. Fernández-Hurtado, F. J. Garcia-Vidal, A. García-Martín, and J. C. Cuevas, Phys. Rev. B 92, 125418 (2015).
- [37] S. Denisov, S. Flach, and P. Hänggi, Phys. Rep. 538, 77 (2014).
- [38] Z. Liao, W. T. M. Irvine, and S. Vaikuntanathan, Phys. Rev. X 10, 021036 (2020).
- [39] U. Seifert, Rep. Prog. Phys. 75, 126001 (2012).
- [40] A. Mogilner and G. Oster, Biophys. J. 71, 3030 (1996).
- [41] F. Jülicher, A. Ajdari, and J. Prost, Rev. Mod. Phys. **69**, 1269 (1997).
- [42] P. Reimann, Phys. Rep. 361, 57 (2002).
- [43] C. O. Reichhardt and C. Reichhardt, Annu. Rev. Condens. Matter Phys. 8, 51 (2017).
- [44] R. P. Feynman, R. B. Leighton, and M. Sands, *The Feynman Lectures on Physics* (Basic Books, New York, 2011), Vol. 1.
- [45] L. Fan, Y. Guo, G. T. Papadakis, B. Zhao, Z. Zhao, S. Buddhiraju, M. Orenstein, and S. Fan, Phys. Rev. B 101, 085407 (2020).
- [46] A. Ishimaru, *Electromagnetic Wave Propagation, Radiation, and Scattering: From Fundamentals to Applications* (John Wiley & Sons, New York, 2017).
- [47] In the opposite limit of $|x| \to \infty$, $g(x) \to (\log |x|)/2$.
- [48] W. G. Spitzer, D. Kleinmann, and D. Walsh, Phys. Rev. 113, 127 (1959).
- [49] The force in Fig. 3 is found to change sign at a distance of several tens of μ m, an effect we leave to future work.
- [50] C. Van den Broeck and R. Kawai, Phys. Rev. Lett. 96, 210601 (2006).
- [51] A. I. Volokitin and B. N. J. Persson, Rev. Mod. Phys. 79, 1291 (2007).
- [52] V. A. Golyk, M. Krüger, and M. Kardar, Phys. Rev. B 88, 155117 (2013).
- [53] $\tilde{\delta}$ is a small window function of finite height and integral of unity.